Observation of Apoptosis and Bone Lamella Structures in the Human Mastoid

Fujiyama, Daisuke*; Yamamoto-Fukuda, Tomomi†‡; Sibata, Yasuaki§; Ikeda, Tohru§; Takahashi, Haruo†

*Department of Otolaryngology, Head and Neck Surgery, Nagasaki University Hospital;
†Department of Otolaryngology, Head and Neck Surgery, ‡Histology and Cell Biology, and §Department of Oral Pathology and Bone Metabolism, Nagasaki University Graduate School of Biomedical Sciences, Nagasaki, Japan

Address correspondence and reprint requests to Daisuke Fujiyama, M.D., Department of Otolaryngology, Japanese Red Cross Nagasaki Genbaku Hospital, 3–15, Mori-mach, Nagasaki 852–8511, Japan
E-mail:dai4795@da2.so-net.ne.jp

The authors disclose no conflicts of interest.

Structured Abstract

Hypothesis: To investigate the localization of apoptotic cells and the lamellar bone structure in mastoid bone tissue, focusing on the mechanism of the development of mastoid pneumatization in humans.

Background: The biological mechanism of poor development of the mastoid air cells found in patients with otitis media (OM) has not yet been fully clarified, as there have been few immunohistochemical research studies to examine the cell biology involved.

Methods: We evaluated the localization of apoptotic cells and the lamellar bone structure in 112 human mastoid bones harvested during various ear surgeries from 57 patients with OM and 55 patients without OM. We used the TdT-mediated dUTP nick end-labeling (TUNEL) method and a polarizing microscope for observing the apoptotic cells and lamellar bone structure, respectively.

Results: The TUNEL-positive cell ratio in an arbitrary 500 cells in the specimen (apoptotic index: AI) was 13.8 in the normal group and 1.2 in the OM group (Mann-Whitney U test, $p<0.001$). From their localization, these apoptotic cells were considered to be osteocytes. The observation of lamellar structures revealed many eroded surfaces in the circumference of the appositional bone in the normal group. In contrast, apposition of bone without an eroded surface was evident in the bone circumference in the OM group.

Conclusion: Apoptosis of osteocytes was significantly suppressed in the mastoid bone of the OM patients. Apoptotic osteocytes may be one of the signals of bone resorption in the process of development of the mastoid air cells. The lamellar structure of the mastoid bone suggested that poor development of the mastoid air cells was caused by decreased resorption of

the appositional bone.

Introduction

In addition to the eustachian tube, the pneumatized mastoid air cells play an important role in regulating middle-ear (ME) pressure. This function is known as transmucosal gas exchange, and it contributes to the maintenance of the physiological condition of the ME [1]. Mastoid air cells grow rapidly in humans until about the age of 5, from that point growth gradually slows until the size plateaus around the age of 15 [2][3].

It is generally known that chronic mastoid inflammation occurring early in life inhibits the development of the ME air cell system [4][5]. There have been many reports observing this phenomenon on computed tomography (CT) or X-ray. In experimental studies using pigs, Ikarashi et al. [6] demonstrated that pneumatized mastoid air cells developed through bone resorption by osteoclasts. They also observed that the decrease in the osteoclasts was observed more often in animals in which mastoid pneumatization is inhibited due to otitis media (OM) than in normal animals. It also has been suggested that mastoid air cells are reduced as a result of bone sclerosis caused by repeated or chronic inflammation [7][8]. However, the biological mechanism of inhibition in pneumatized mastoid air cells found in patients with OM has not yet been fully clarified, as there have been few immunohistochemical research studies to examine the cell biology involved.

Palva et al. [9] reported that the mesenchyme adjoining the petrous bone contained more apoptotic cells than those in the tympanic and epitympanic regions in young fetuses. Roberts et al. reported that apoptotic cells were found within the mesenchyme along the superior cavitating edge of the middle ear space in 8 mouse pups [10]. Matsuo et al. reported that osteocytic apoptosis becomes the control factor that is important to both bone resorption and formation [11]. These data suggested that apoptotic cells may be related to the pneumatization process. To date, however, there has been no report examining the apoptotic cells in human mastoid tissue.

In this study, in order to obtain a clue to clarify the process of mastoid

pneumatization and its inhibition by OM in human, we examined apoptotic cells in the human mastoid bone and lamellar structure of bone surface around the human mastoid air cells. Apoptotic cells were defined as TdT-mediated dUTP-biotin nick end-labeling (TUNEL) staining-positive cells, and lamellar structure was evaluated by the structure of osteon (an element of Haversian canal and circumferential lamellar bone) under a polarizing microscope on the basis of resorption of a part of circumference of osteons and apposition of new bone on the eroded surface.

Materials and methods

1. Subjects

The subjects were 112 patients who underwent various ear surgeries in the Department of Otolaryngology, Nagasaki University Hospital from June 2005 to July 2009. Their mastoid bone tissues were obtained through mastoidectomy. The subjects were divided into two groups. The normal group consisted of patients who had normal mastoid air cell growth without history of OM prior to surgery and who underwent ear surgery, such as a cochlear implantation (CI) as described later. The OM group consisted of patients with cholesteatomatous OM and non-cholesteatomatous OM with tympanic membrane perforation and OM with effusion, along with suppressed mastoid pneumatization or sclerotic mastoid with granulation tissue filling the mastoid space. They underwent ear surgery, such as tympanoplasty with mastoidectomy or CI as described later. The mastoid pneumatization was assessed by using an axial image of the high-resolution CT on the level at which the lateral semicircular canal can be seen most clearly. When mastoid pneumatization was suppressed or the mastoid was filled with soft tissue density as confirmed by CT, it was judged as suppressed pneumatization or sclerotic mastoid. It was defined as normal pneumatization when the mastoid pneumatization was good without soft tissue density as confirmed by CT.

Sufficient explanation was given to all of the patients, and written informed consent was obtained from all of the patients or their guardians. This study was approved by the ethical committee of our institute (Approval Number 06092284). Temporal bone specimens were obtained during surgery on 112 patients. 79 out of 112 specimens, were cut serially and used for TUNEL staining or observation of the lamella structure under a polarizing microscope, and 33 out of 112 specimens were homogenized and used for western blot analysis. The specimens used for the details of subjects were described below.

(1) TUNEL staining

The staining was done on 79 specimens from 79 patients; 39 from the normal group and 40 from the OM group. The normal group consisted of 18 males and 21 females ranging in age from one to 80 years (average: 17 years). Thirty-two patients underwent cochlear implantation (CI), 4 had acoustic neuroma, 2 external auditory canal (EAC) cholesteatoma, and the remaining one had traumatic ossicular disruption. The OM group consisted of 18 males and 22 females ranging in age from 2 to 75 years (average: 42 years). Thirty four patients had cholesteatomatous OM (pars flaccida cholesteatoma 24 cases, pars tensa cholesteatoma 10 cases), 5 had non-cholesteatomatous chronic OM with tympanic membrane perforation, and the remaining one patient underwent CI surgery but had chronic OM with effusion (OME).

(2) Western blot analysis for FAS

This analysis was done on 33 specimens from 33 patients; 16 from the normal group and 17 from the OM group. The normal group consisted of 6 males and 10 females ranging from one to 68 years (average: 15 years). Thirteen patients underwent CI, one had acoustic neuroma, and the remaining 2 had EAC cholesteatoma. The OM group consisted of 6 males and 11 females ranging in age from one to 79 years (average: 41 years). Thirteen

patients had cholesteatomatous OM (pars flaccida cholesteatoma 9 cases, pars tensa cholesteatoma 4 cases), and the remaining 4 had non-cholesteatomatous OM with tympanic membrane perforation.

(3) Observation of the lamellar structure under a polarizing microscope

This analysis was done on specimens from 40 patients; 19 from the normal group and 21 from the OM group. The normal group consisted of 11 males and 8 females ranging in age from one to 17 years (average: 5 years). Sixteen patients underwent CI, one had EAC cholesteatoma, one had traumatic ossicular disruption, and the remaining one had traumatic tympanic membrane perforation. The OM group consisted of 9 males and 12 females ranging in age from one to 75 years (average: 37 years). Eighteen patients had cholesteatomatous OM (pars flaccida cholesteatoma 15 cases, pars tensa cholesteatoma 3 cases) and the remaining 3 had non-cholesteatomatous OM with tympanic membrane perforation.

2. Preparation of tissues and methods

(1) TUNEL staining

The mastoid bone tissues were harvested as a cylindrical-shaped block that contained both the cortex and the air cells adjacent to the mastoid antrum. The bone tissues were stored at -84 degrees centigrade (^{o}C) to produce frozen sections. The bone tissues were frozen in a cooled hexane or liquid nitrogen and then freeze-embedded with 4-5% carboxymethyl cellulose (CMC) in the coolant. An adhesive film was fastened to the cut surface of the sample to support the section and the bone tissue cut with a tungsten carbide blade with cryomicrotome equipment [12]. Four-μm-thick sections were mounted on glass slides by adhesion film (cryofilm type 2C FINETEC).

To analyze DNA fragmentation in histological sections, TUNEL staining was carried out according to the method of Gavrieli et al. [13] with a slight modification, as described below [14][15]. The bone tissues were fixed

in 4% paraformaldehyde for 10 minutes. Tissue sections were digested with 10ng/ml proteinase K (PK) (Wako Pure Chem. Co., Japan) in PBS for 15 minutes (min.) at 37°C, and the slides washed three times in PBS for 5 min. each.

After preincubation with terminal deoxynucleotidyl transferase (TdT) buffer (pH 6.6) consisting of 200 mM potassium cacodylate, 25 mM Tris-HC1 and 0.25 mg/ml BSA (Roche) alone for 30 min., sections were further reacted with TdT for another 90 min. at 37°C in a medium containing the TdT buffer, 20 μM dATP, 0.1 mM DTT, 1.5 mM cobalt chloride, 0.2 U/μl TdT and 0.5 μM biotinylated 16-dUTP (Roche). The reaction was terminated by transferring the slides to 50 mM Tris-HCl buffer (pH 7.4), which were then washed three times for 5 min. each with 50 mM Tris-HCl buffer, followed by rinsing with PBS.

Endogenous peroxidase was inactivated by immersing the sections in 0.3% H2O2 in methanol for 15 min., followed by washing three times with PBS for 5 min. each. After incubation with 500 μg/ml normal goat IgG in 5% BSA-PBS for 60 min., sections were incubated with horseradish peroxidase (HRP)-goat anti-biotin (Vector Laboratories, Burlingame, California, USA) (1:100) diluted with 5% BSA in PBS for overnight at room temperature (RT), and washed four times, for 15 min. each, with 0.075% Brij 35-PBS. 3,3'-Diaminobenzidine-4HCl and H_2O_2 were used to visualize HRP sites.

As a negative control, some sections were treated with Milli-Q water instead of TdT. Finally, the slides were dehydrated with serial ethanol solutions, cleared with xylene, and mounted using standard procedures without counter-staining.

TUNEL-positive cells, which were not located in the submucosal layer but in the mastoid bone tissue, were observed under the light microscope and counted to calculate the apoptotic index (AI), which indicates the ratio in percentage of apoptotic cells in the 500 cells found in the mastoid bone.

(2) Western blot analysis for Fas

Mastoid bone tissues (500mg) were homogenized with a Freeze triturator tool (Tokken Inc., Tokyo, Japan) in lysis buffer (20mM Tris-HCI, pH 7.4, 1.0 M NaCl, 5mM EDTA, 1mM phenylmethylsulfonylfluoride, 10μg/ml aprotinin, 10 μg/ml leupeptin, 10% glycerol, and 0.5% Triton X-100) on ice [16][17]. After centrifugation at 15,000 rpm for 3 min. at 4°C, the supernatants were collected and mixed with protease inhibitor. The protein concentration of each preparation was determined using a kit from PIERCE (USA) according to the instructions provided by the manufacturer, using BSA as a standard. In the next step, 50μg of sample lysates and the recombinant proteins were mixed with the loading buffer (2.5% SDS, 200 mM Tris-HCl, pH 8.0, 0.5 M sucrose, 5 mM EDTA, 0.01% bromophenol blue, and 429 mM 2-mercaptoethanol), and loaded on each lane.

Samples were separated by SDS-PAGE with a 12.5% gradient gel (Bio-Rad Laboratories, Tokyo, Japan) according to the method of Laemmli [18], and were electrophoretically transferred to a PVDF membrane (Bio-Rad Laboratories). The membranes were blocked with PBS containing 5% nonfat dry milk and 5% BSA overnight at 4°C and then incubated for 2 hours with the first antibody (0.005μg/ml purified mouse anti-Fas) with the blocking solution. After washing, the membranes were reacted with ECL-anti-mouse IgG (GE Healthcare) at a 1:1,000 dilution as the second antibody for 90 min. at RT. Finally, signals were visualized using X-ray film. The staining intensities were graded as negative (-) or positive (+) in each case.

(3) Observation of the lamellar structure under a polarizing microscope

A frozen section 4-μm-thick was produced without decalcifying in the same way as that for TUNEL staining. The present study was undertaken to observe the lamellar structure of the bone surface around the mastoid air cells, particularly on the surfaces of bone apposition and resorption, under a polarizing microscope. The length was measured in terms of (1) the eroded

surface (the surface on which the lamellar structure had become interrupted, i.e., the surface on which the bone had been eroded by osteoclasts (Fig. 1B, C)), and (2) the surface of bone apposition (the surface on which the lamellar structure is arranged in parallel, i.e., the surface of bone apposition with osteoblasts) (Fig. 1) [19] [20] [21]. The ratio in percentage of the eroded surface to the bone circumference (E/C ratio) was calculated in each case, and was compared between the normal and OM groups.

Statistical analysis

Statistical analyses were performed on a personal computer with the StatView for Windows (Version 4.51; Abacus Concepts, Berkeley, California, USA). AI was analyzed by Mann-Whitney U test; Western blot studies were analyzed by Fisher's exact test. Observation of the lamellar structure was analyzed by Student's T test. A p-value of less than 0.05 was considered statistically significant.

Results

1. TUNEL staining

Figure 2 shows the TUNEL staining of the mastoid bone of a representative case in the normal group. Her preoperative CT showed normal mastoid air cell growth. Many TUNEL-positive cells were found in the bone tissue at the margin of the air cells (Fig. 2A). Observation at higher magnification of the same case in the normal group showed many TUNEL-positive cells in the bone tissue adjacent to the mastoid air cell, as well as in the osteocyte lacuna (Fig. 2B). The results of H&E staining (Fig. 2C) and von Kossa staining (Fig. 2D) in the serial sections showed that TUNEL-positive cells were most likely osteocytes.

Whereas, a representative case in the OM group showed no TUNEL-positive cell in the mastoid bone tissue on the air-cell side (Fig. 3). His preoperative CT showed a poorly developed mastoid that was filled with soft

tissue densities.

2. Comparison of AI

Subjects were divided into two groups in this study. One included patients 14 years of age or younger (younger group); the other included subjects age 15 or older (older group). In the normal group, AI was significantly higher in the younger group (mean±SD = 18.3±13.3, n=28) than in the older group (2.3±3.4, n=12) (P=0.001, Fig. 4). These results seem to suggest that apoptosis of the mastoid bone cells is prevalent during the period of growth of mastoid pneumatization in normal subjects.

On the other hand, in comparing between the normal and OM groups in the younger group, AI was significantly higher in the normal group (18.3±13.3, n=28) than in the OM group (4.45±6.8, n=9, P=0.005), suggesting that apoptosis may be suppressed in an environment of inflammation.

3. Western blot analysis of Fas

As shown in Fig. 5, a 45 kDa band was detected in the extracts of cases with normal mastoid (lane 2, 3) by anti-Fas antibody. On the other hand, a 45 kDa band was not detected in the extracts of the non-cholesteatomatous OM with tympanic membrane perforation (Fig. 5, lane 4) and cholesteatomatous OM (Fig. 5, lane 5). But in the extracts from some samples of the OM group, a 45 kDa band was detected (Fig. 5, lane 6). In the normal group (n=16), the positive rate of Fas was 87.5%, while in the OM group (n=17), it was 47.1%. The difference was statistically significant between the two groups (Fisher's exact test: P=0.025), indicating that activity related to apoptosis seemed to take place more often in the normal group than in the OM group.

4. Observation of the lamellar structure under a polarizing microscope

Figure 6 shows a photograph of a mastoid bone of a representative

case (a 17-year-old girl) in the normal group. Her mastoid air cell was found to be well developed (Fig. 6A). When observed under a polarizing microscope, her mastoid bone showed prominent lamellar structures (primary lamellar bone) running unidirectionally with few osteon structures (Fig. 6B). There were also many break (cutting) surfaces of the lamella, namely an eroded surface, and the ratio of eroded surface to bone circumference was found to be as high as 78% in this case.

Figure 7 shows a photograph of the mastoid bone of a representative case in the OM group (a 10-year-old girl with cholesteatoma), as observed under a polarizing microscope. Her preoperative temporal bone CT showed a poor and sclerotic mastoid that was occupied mostly by the bone matrix and few air cells (Fig. 7A). When observed under a polarizing microscope, there was a more complex structure made of overlaps of osteon and lamellar bone (Fig. 7B), indicating the outcome of repeated cycles of bone remodeling [20]. The ratio of bone apposition to bone circumference accounted for as much as 60%, and the ratio of bone eroded surface was found to be 25% in this case, suggesting that bone apposition is greatly influenced by bone formation. These results indicate that, in cases with mastoid inflammation, osteoblasts may contribute greatly to new bone formation.

Figure 8 shows a photograph of an atypical case with normal mastoid growth but with a cholesteatoma (9-year-old girl). Her preoperative temporal bone CT showed normal mastoid growth (Fig. 8A), but during surgery a cholesteatoma was found in the attic, tympanum, and mastoid antrum with inflammatory effusion in the mastoid. Under a polarizing microscope (Fig. 8B), both complicated lamination frequently seen in the inflammation case and the unidirectional lamination frequently seen in a normal case were mixed. The ratio of bone eroded surface to bone circumference accounted for 58.1% in this case. The development and population of air cells were found to be almost the same as in a normal case, but a complex structure characterized by protrusion of lamellar bone into the mastoid air cell was

noted to be unlike a normal case, showing an area having evidently undergone additional ossification. In other words, it was speculated that the apposition portion was added as a result of chronic inflammatory stimulation of the normal air cell structure.

The E/C ratio was more than 59 with an average of 73.33±8.69 in all of the normal cases. In the OM group, it was less than 58 in all of the cases with an average of 25.35±19.60, thus being significantly lower in this group (Fig 9, Student's t-test, $P<0.001$). Based on these results, it is suggested that the contribution of osteoclasts was greater in a normal case than in an OM case, whereas the contribution of bone apposition by osteoblasts may become eminent in an OM case. Another interesting finding was that in the OM group, the ratios were smaller in those older than 15 years of age than in those younger than 15 (Student's t-test, $p=0.009$), and also that the values of the 6 cases younger than 15 were all greater than the average of those older than 15 years of age.

Discussion

The bone matrix has a specific lamellar structure. When bone is formed or remodeled, concentric lamellar structures around the blood vessels are regularly created [21]. Observation of such lamellar structures provides information about the status of remodeling, such as bone sclerosis and ossification by osteoblasts, and/or bone resorption by osteoclasts, thus enabling observation of the overall aspects of the cell activities that constitute bone tissue [21]. As one of the characteristic findings on the surface of the mastoid bone facing toward the mastoid air cells, a high percentage of erosion was noted in the normal group. In the normal group, most subjects underwent CI, and many of them were at an age when the mastoid air cell structure was vigorously expanding. It seems likely that osteoclasts are involved at the ages at which the normal mastoid air cell structure is usually developing, and this is compatible with previous reports [6, 22].

In the OM group, there was a more complex structure constructed of overlaps of osteon and lamellar bone, indicating an outcome of repeated cycles of bone remodeling [21]. In the OM cases, chronic inflammation may stimulate bone metabolism more than in the normal cases, resulting in repeated cycles of remodeling. In a case of OM showing relatively well-developed mastoid pneumatization (Fig. 8), a complex structure characterized by the protrusion of lamellar bone into the mastoid antrum was noted, evidently showing an area having undergone additive ossification. This represents the replacement of mastoid air cells by bone matrix following bone apposition due to chronic inflammation, which occurred after the pneumatization was once formed. Furthermore, the E/C ratios were smaller in those older than 15 years of age than in those younger than 15 years (Fig. 9), indicating that the remodeling and additive ossification in the mastoid bone may be even more frequent at a more advanced age in OM patients. This seems to reflect the mechanism of sclerotic change of the air cells in patients with chronic inflammation, probably presenting with a decrease in the area of the mastoid.

The present study revealed that mastoids with well-developed, normal air cells were rich in TUNEL-positive osteocytes, while TUNEL-positive osteocytes were rarely present in the mastoids with poorly developed air cells that were seen in the OM group. The first biochemical change of apoptotic cells is a double-strand break of genomic DNA. The TUNEL staining method detects the site of the double-strand break immunohistologically, and it can be observed using an optical microscope [13]. According to one report [23], it is not possible to draw a definite conclusion about apoptotic cells on the basis of TUNEL staining alone. In the present study, we attempted to detect Fas for an auxiliary diagnosis. Apoptosis is considered to have two major signal pathways: the mitochondrial pathway and the death receptor pathway [24]. Fas is a death receptor and has an apoptosis-related protein on the cell structure. According to the results of the

present study, the Fas-positive rate was found to be significantly higher in the normal group than in the OM group. This seems to well agree with the results of the TUNEL positive rate, and we defined TUNEL-positive osteocytes as apoptotic osteocytes.

Matsuo et al. reported that osteocytes have a network that involves osteoblasts and osteoclasts, and that apoptosis of osteocytes leads to differentiation and induction of osteoclasts [11]. Another report also suggested that apoptosis of osteocytes is an important signal and plays a significant role in the start of bone metabolism [25]. The results of the present study suggest that apoptosis of osteocytes plays a significant role in the developed mastoid, and also provides signals to induce and activate the osteoclasts that are involved in bone resolution and the formation of cavities in the mastoid. Whereas, apoptosis of osteocytes is assumed to be suppressed by mastoid inflammation, and this may lead to suppression of bone metabolism, including the activity of osteoclasts responsible for creating the mastoid air space. It has been reported that apoptosis of osteocytes is induced by glucocorticoids [26]. Therefore, it may be possible that local or general administration of glucocorticoid may be effective in preventing the inhibition of pneumatization due to inflammation in the mastoid. Further studies should be conducted to clarify the cell-biological mechanism by which apoptosis is suppressed when there is inflammation in the mastoid.

In conclusion, the biological mechanisms involved in the poor air cell development in the mastoids of OM patients have long been studied and two hypotheses have been proposed. One is decreased bone resorption and the other is increased osteogenesis. However, direct biological evidence has not been reported, largely because of the difficulties inherent in biologically analyzing the sclerotic mastoid. In this study, we analyzed subjects' mastoids using undecalcified frozen sections and polarized microscopy. Detection of apoptotic cells and analyses of the lamellar structures of the bone suggested that poor air cell development in the mastoids was caused by apposition of

the bone into the air cells and the reduced resorption of appositional bone, and that resorption may be regulated by apoptotic osteocytes.

References

1) Takahashi H. Middle-ear physiology: ventilation and pressure regulation. In The Middle Ear – The Role of Ventilation in Disease and Surgery, ed by Takahashi H. Tokyo: Springer-Verlag, 2001. 1-18.

2) Rubensohn G. Mastoid pneumatization in children at various ages. Acta Otolaryngol 1965;60:11-14.

3) O'Donoghue GM, Jacker RK, Jenkins WM, et al. Cochlear implantation in children: the problem of head growth, Otolaryngol Head Neck Surg 1986;94:78-81.

4) Diamant M. Pneumatization of the mastoid bone. J Laryngol Otol 1958; 2:343-364.

5) Turmarkin A. On the nature and significance of hypocellularity of the mastoid, J Laryngol Otol 1959;73:34-44.

6) Ikarashi F, Nakao Y, Okura T. The relationship between the degree of chronic middle ear inflammation and tympanic bulla pneumatization in the

pig as animal model. Eur Arch Otorhinolaryngol 1994;251:100-104.

7) Friedmann I. The pathology of otitis media (III) with particular reference to bone changes. J Laryngol Otol 1957;71:313-320.

8) Caye-Thomasen P, Hermansson A, Tos M, et al. Bone modeling dynamics in acute otitis media, Laryngoscope 1999;109:723-729.

9) Palva T, Pääkkö P, Ramsay H, Chrobok V, et al. Apoptosis and regression of embryonic mesenchyme in the development of the middle ear spaces. Acta Otolaryngol 2003;123:209-214.

10) Roberts S, Miller S. Apoptosis in cavitation of middle ear space. Anat Rec 1998;251:286-289.

11) Matsuo K, Irie N. Osteoclast-osteoblast communication. Archives of Biochemistry and Biophysics 2008;473:201-209.

12) Kawamoto T. Use of a new adhesive film for the preparation of multi-purpose fresh-frozen sections from hard tissues, whole-animals, insects and plants. Arch Histol Cytol 2003;66:123-143.

13) Gavrieli Y, Sherman Y, Ben-Sasson SA. Identification of programmed cell death in situ via specific labeling of nuclear DNA fragmentation. J Cell Biol 1992; 119:493-501.

14) Koji T. Nonradioactive in situ nick translation: a useful molecular histochemical tool to detect single-stranded DNA breaks. Acta Histochem Cytochem 1996; 29:71-79.

15) Wang RA, Nakane PK, Koji T. Autonomous cell death of mouse male germ cells during fetal and postnatal period. Biol Reprod 1998; 58:1250-1256.

16) Koji T, Chedid M, Rubin JS, et al. Progesterone-dependent expression of keratinocyte growth factor mRNA in stromal cells of the primate endometrium: Keratinocyte growth factor as a progestomedin. J Cell Biol 1994;125:393-401.

17) Wilson SE, Liang Q, and Kim WJ. Lacrimal gland HGF, KGF and EGF mRNA levels increase after corneal epithelial wounding. Invest Ophthalmol

Vis Sci 1999;40:2185-2190.

18) Laemmli UK. Cleavage of structural proteins during the assembly of the hand of bacteriophage T4. Nature 1970;227:680-685.

19) Eriksen EF, Axelrod DW, Melsen F. Bone Histomorphometry. New York: Raven Press, 1994.13.

20) Parfitt AM. The cellular of bone remodeling: the quantum concept reexamined in light of recent advances in the cell biology of bone. Calcif Tissue Int 1984;36:37-45.

21) Suda T, Ozawa H, Takahashi H, et al. Bone Biology. Tokyo: Ishiyaku Publishers, 2007.17-27.

22) Aoki K, Esaki S, Honda Y, et al. Effect of middle ear infection on pneumatization and growth of the mastoid process. An experimental study in pigs. Acta Otolaryngol 1990;110:399-409.

23) Hengartner MO. The biochemistry of apoptosis. Nature 2000;12:770-776.

24) Hakuno N, Koji T, Yano T, et al. Fas/APO-1/CD95 system as a mediator of

granulose cell apoptosis in ovarian follicle atresia. Endocrinology 1996;137:1938-1948.

25) Henriksen K, Neutzsky-Wulff AV, Bonewald LF, et al. Local communication on and within bone controls bone remodeling. Bone 2009;44:1026-1033.

26) Weinstein RS, Nicholas RW, Manolagas SC. Apoptosis of osteocytes in glucocorticoid-induced osteonecrosis of the hip. Clin Endocrinol Metab. 2000;85:2907-2912.

Figure legends

Figure 1. The bone surface of a normal mastoid air cell as observed by a polarizing microscope. A. The surface on which the lamellar structure has become interrupted by erosion by osteoclasts (eroded surface) is shown by arrowheads. The surface on which the lamellar structure is arranged in parallel by the apposition with osteoblasts (bone apposition surface) is shown by arrows. Asterisk: mastoid air cell. Black bar: 100 um. B. Higher magnification of the eroded surface. C. H&E staining in the same section of fig. 1B. The osteoclast on the eroded surface is shown by black arrowhead. White bars: 10 um.

Figure 2. A. TUNEL staining of the mastoid bone of a subject in the normal group (3-year-old girl). The expression of TUNEL-positive cells were mostly confined to the periphery of the bone tissue. Bar: 50 um. B. Higher magnification of TUNEL staining in the mastoid bone section (see box, fig.2A). Bar: 20 um. C. H&E staining of serial section. D. von Kossa staining of serial section. Bone structure was detected in the area of TUNEL positive cells were shown. The results of Fig 2B, C, D indicated that TUNEL-positive cells were most likely osteocytes. Arrows: TUNEL-positive cells. Bar: 20 um. Arrows: TUNEL-positive cells; arrowheads: osteocyte; asterisks: mastoid mucosa.

Figure 3. A. TUNEL staining of the mastoid bone of a subject with OME (OM group, 2-year-old boy). Bar: 50 um. B. Higher magnification (see box, fig. 3A). No TUNEL-positive cells were observed (arrows). Bar: 20 um. Arrows: the nuclei of TUNEL-negative cells.

Figure 4. Apoptotic index. Normal and OM groups were divided into two age groups: 14 years of age and younger and age 15 and older. *: P< 0.01.

Figure 5. The results of western blot analysis of Fas. The total volume of applying is 50μg per lane. All lanes were reacted with 0.005 ug/ml mouse monoclonal anti-Fas antibody. A: Recombinant protein against Jurkat (positive control). B, C: lysate of a subject in the normal group (B: 2-year-old female, C: 16-year-old woman.). D, E, F: lysate of a subject in the OM group (D: non-cholesteatomatous OM with tympanic membrane perforation (30-year-old man), E: cholesteatoma (55-year-old woman), F: cholesteatoma (27-year-old man))

Figure 6. Axial temporal bone CT image (A) and polarizing microscope images (B) of a subject in the normal group (17-year-old girl). Many lamellar structures (primary lamellar bone) are running unidirectionally (asterisks), and few osteon structures are seen (stars). There are many break (cutting) surfaces of the lamella (white arrows), namely an eroded surface, and the ratio of the surface of bone apposition was found to be 21%, while the ratio of the eroded surface was found to be 78%. The subject's temporal bone CT showed good mastoid air cell growth. Bar: 100 um.

Axial temporal bone CT image (A) and polarizing microscope images (B)

Figure 7. Axial temporal bone CT image (A) and polarizing microscope images (B) of a subject in the OM group (10-year-old boy). The mastoid was occupied mostly by the bone matrix, and air cells were few (asterisk). There was a more complex structure with overlaps of osteon and lamellar bone (stars). The ratio of the surface of bone apposition was found to be 60%, while the ratio of eroded bone surface was 25%. The subject's CT showed poor mastoid air cell growth and sclerotic bone changes. Bar: 100 um.

Figure 8. Axial temporal bone CT image (A) and polarizing microscope images (B) of the mastoid bone of a subject (9-year-old girl) not in the normal or OM group. Large air cells (star) and lamellar structures (asterisks) similar to that in a normal case were found. Complex structure characterized by the protrusion of lamellar bone into the mastoid air cell were noted (white arrows), evidently showing an area that had undergone bone apposition. The subject's temporal bone CT showed normal mastoid growth, but cholesteatoma was found in the attic and mastoid antrum with effusion in the mastoid. Bar: 100 um.

Figure 9. Comparison of the ratio of eroded surface to bone circumference (E/C ratio) between the normal (◊) and the OM group (■). Note that the ratios are higher in the normal than in the OM cases (Student's t-test, $p<0.001$), and also that in the OM group, the ratios were smaller in those older than 15 years of age than in those younger than 15 years (Student's t-test, $p=0.009$).

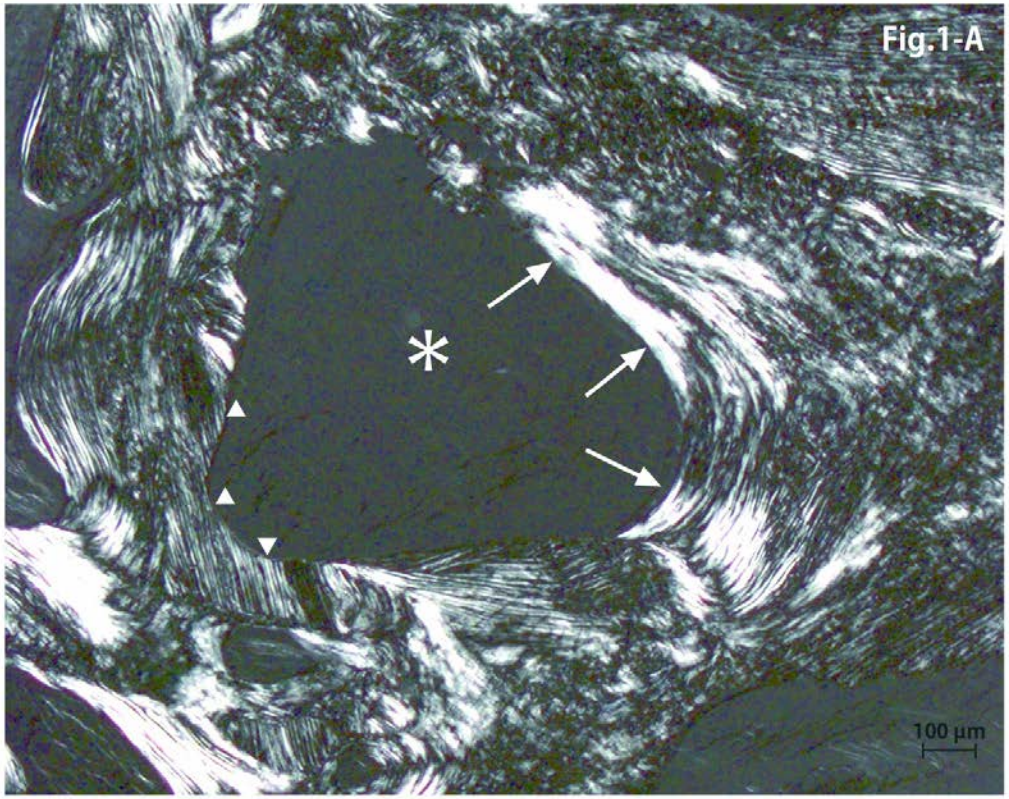
Fig.1-A
100 µm

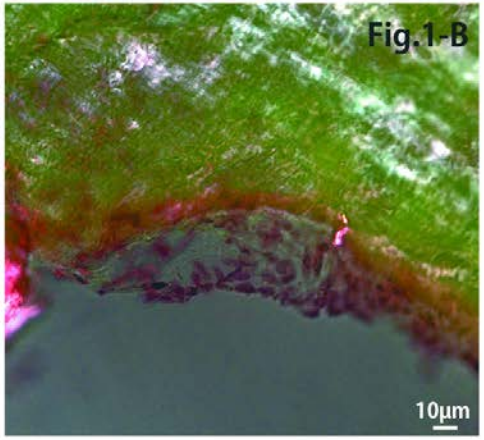
Fig.1-B
10µm

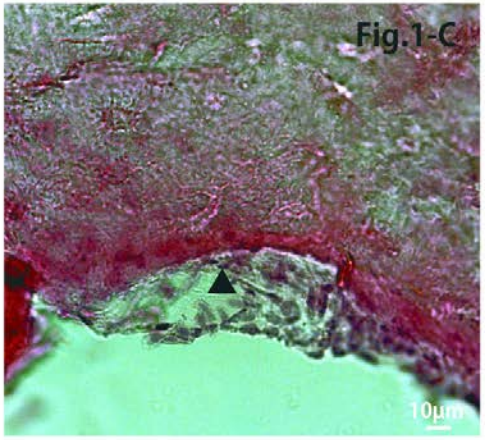
Fig.1-C
10µm

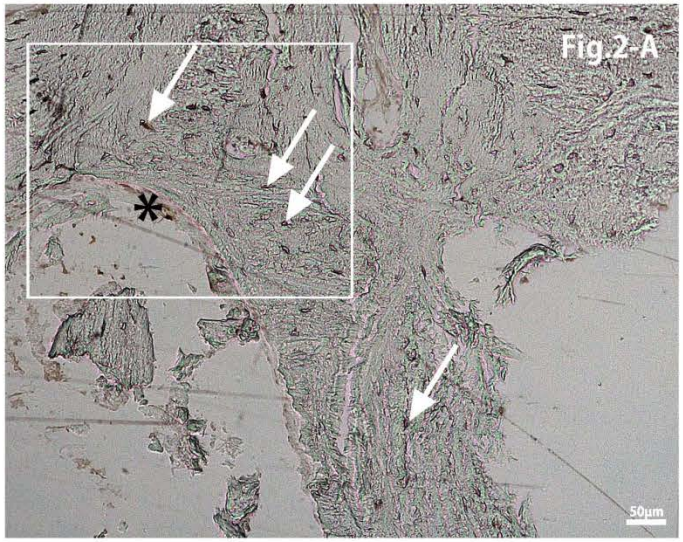
Fig.2-A
50μm

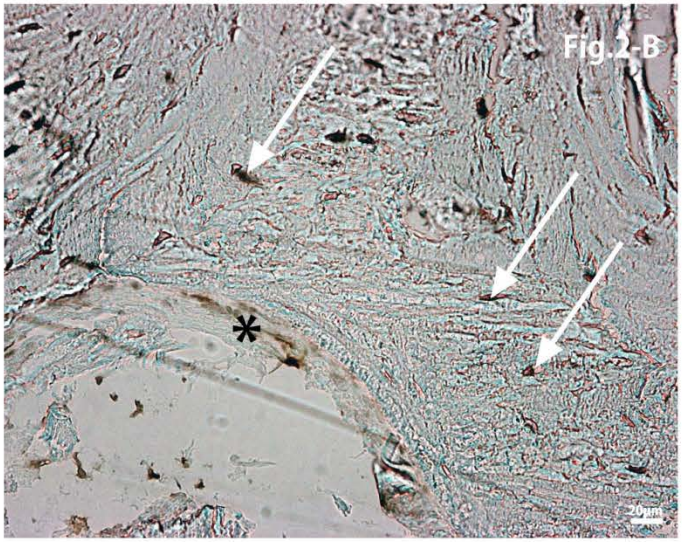
Fig.2-B
20μm

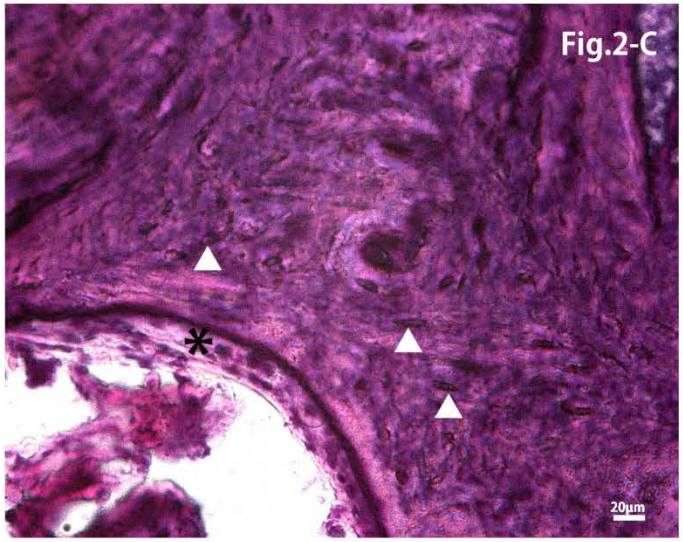
Fig.2-C
20μm


Fig.2-D
20μm

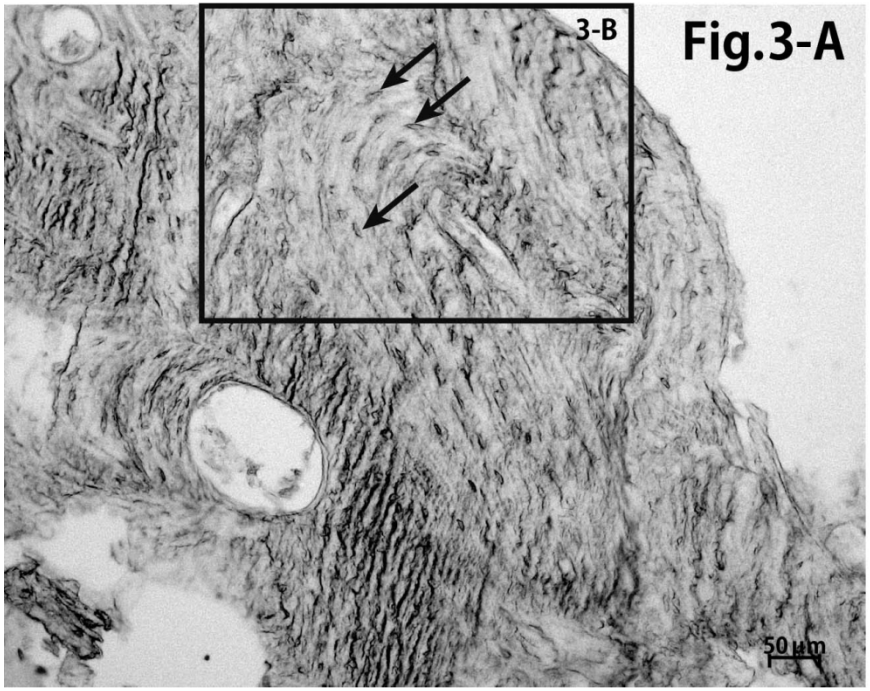
3-B
Fig.3-A
50 µm

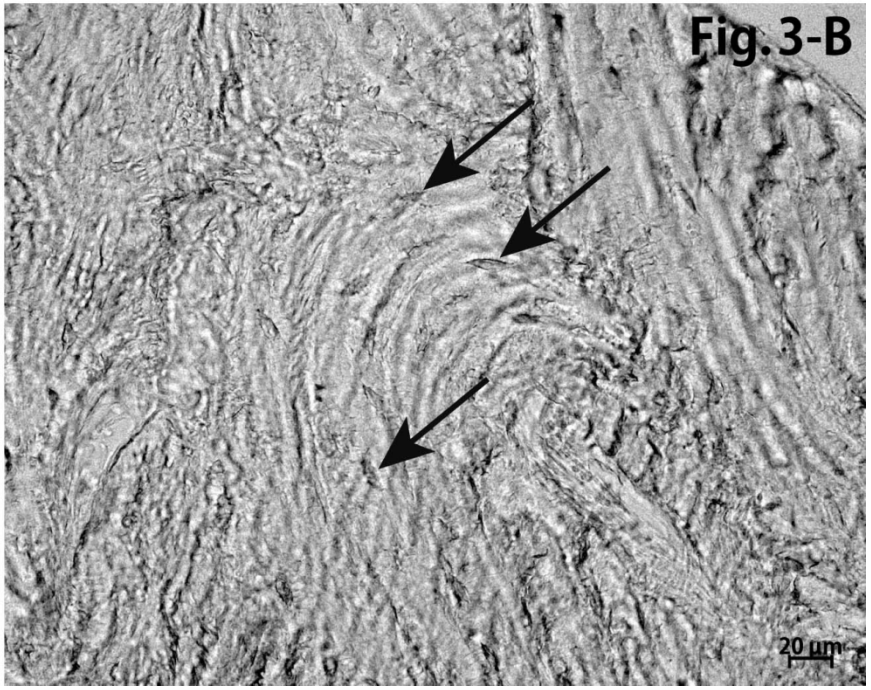
Fig. 3-B
20 µm

Fig.4

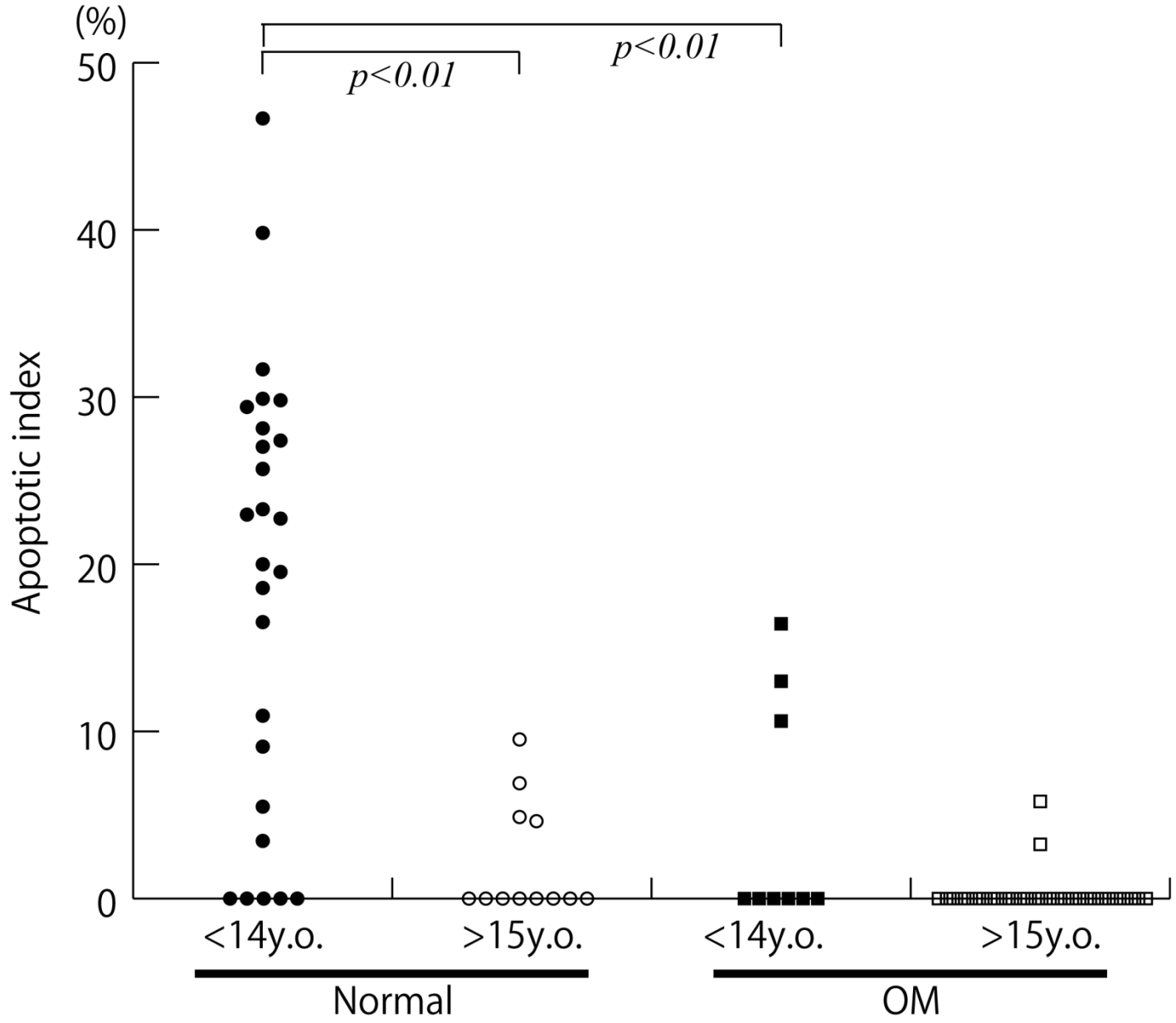
(%)
p<0.01
p<0.01
50
40
30
20
10
0
Apoptotic index
<14y.o.
>15y.o.
<14y.o.
>15y.o.
Normal
OM

Fig.5

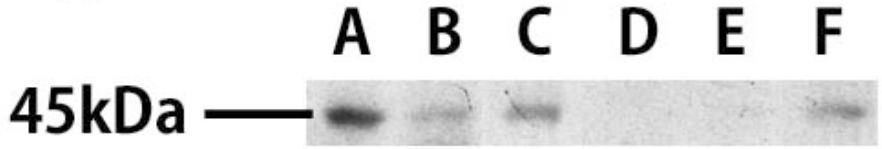


Fig.6-A
INTERP-3/F

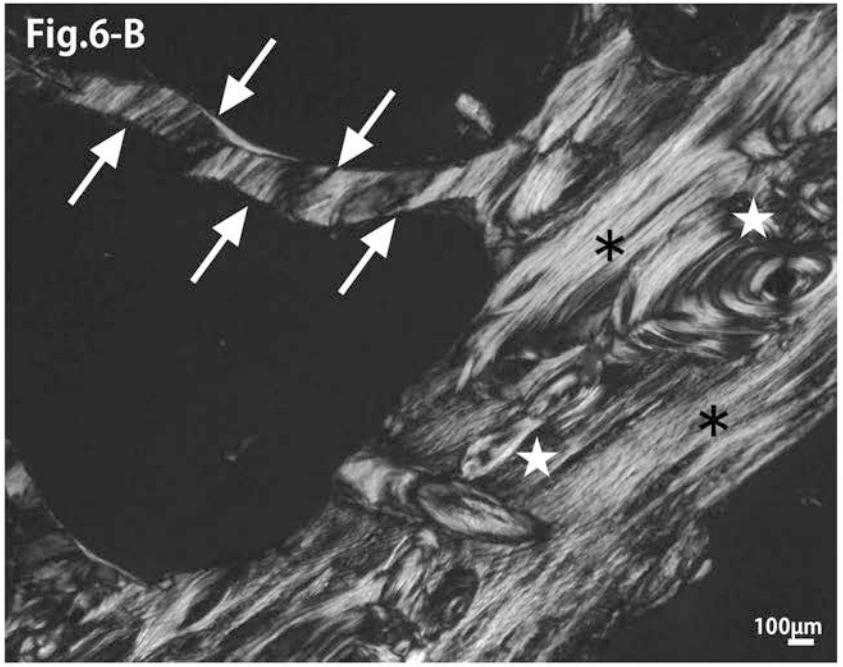
Fig.6-B
100μm


Fig.7-A

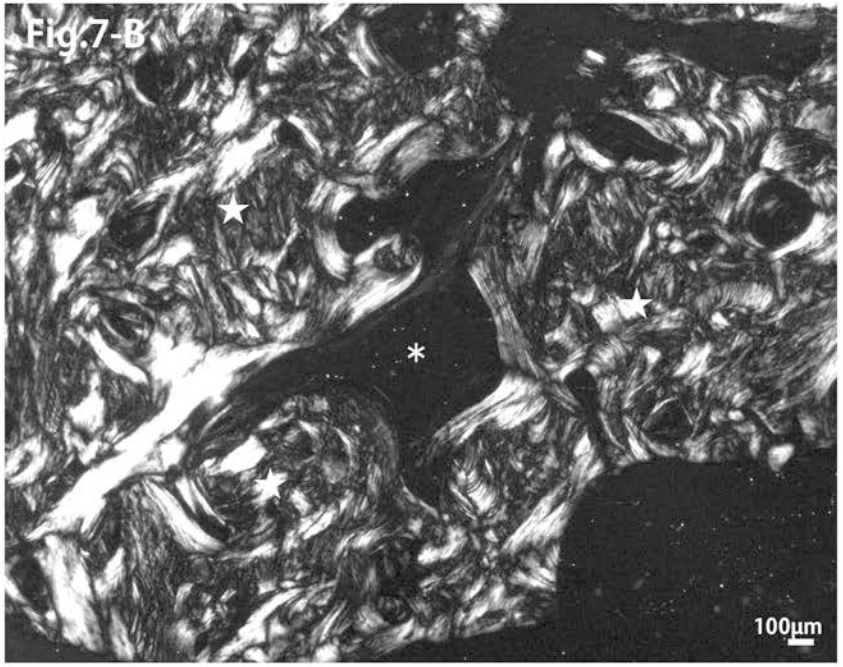
Fig.7-B
100μm


Fig.8-A

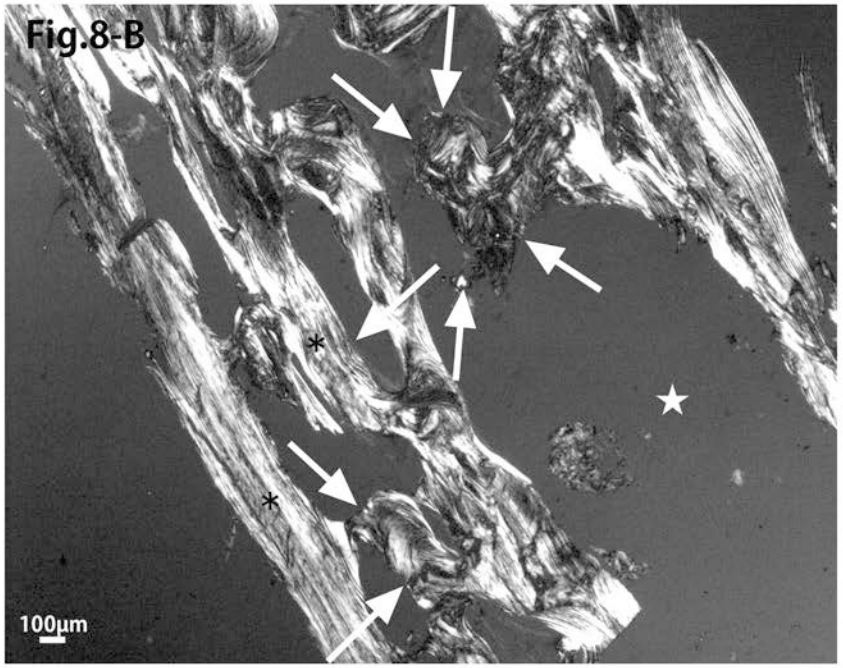
Fig.8-B
100μm

Fig.9